Chemistry–A European Journal
Review
doi.org/10.1002/chem.202400277
Chemistry Europe
European Chemical Societies Publishing
www.chemeurj.org

# Aggregation Mechanisms and Molecular Structures of Amyloid-β in Alzheimer's Disease

Zheng Niu,*[a] Xinrui Gui,[b] Shuang Feng,[a] and Bernd Reif*[c, d]

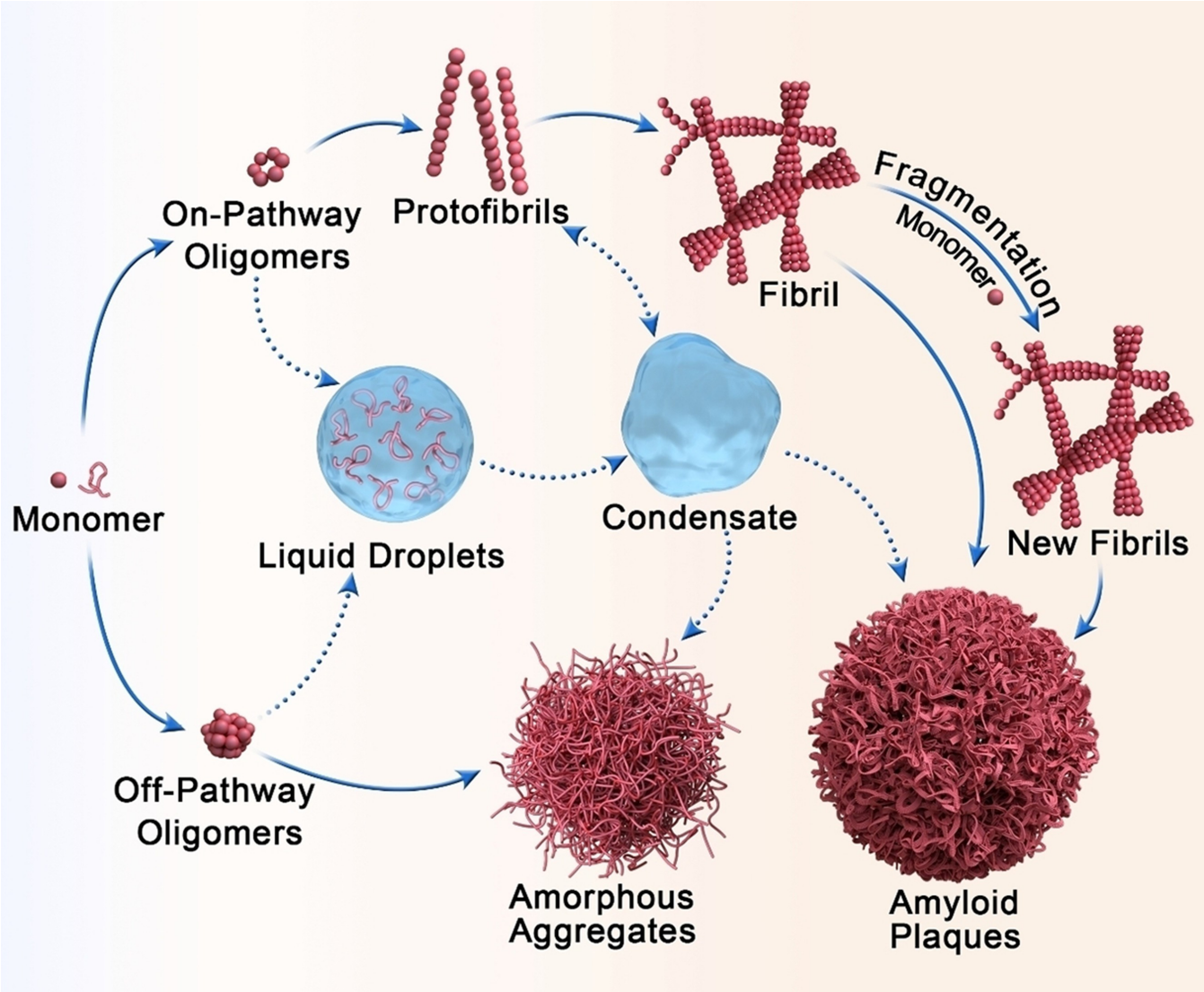



© 2024 The Authors. Chemistry - A European Journal published by Wiley-VCH GmbH

Amyloid plaques are a major pathological hallmark involved in Alzheimer's disease and consist of deposits of the amyloid-β peptide (Aβ). The aggregation process of Aβ is highly complex, which leads to polymorphous aggregates with different structures. In addition to aberrant aggregation, Aβ oligomers can undergo liquid-liquid phase separation (LLPS) and form dynamic condensates. It has been hypothesized that these amyloid liquid droplets affect and modulate amyloid fibril formation. In this review, we briefly introduce the relationship between stress granules and amyloid protein aggregation that is associated with neurodegenerative diseases. Then we highlight the regulatory role of LLPS in Aβ aggregation and discuss the potential relationship between Aβ phase transition and aggregation. Furthermore, we summarize the current structures of Aβ oligomers and amyloid fibrils, which have been determined using nuclear magnetic resonance (NMR) and cryo-electron microscopy (cryo-EM). The structural variations of Aβ aggregates provide an explanation for the different levels of toxicity, shed light on the aggregation mechanism and may pave the way towards structure-based drug design for both clinical diagnosis and treatment.

## 1. Introduction

Alzheimer's disease (AD), as a typical neurodegenerative disease (ND), reportedly affects 50 million people worldwide.[1] Clinically, $<5\%$ of AD cases are the inherited familial form with genetic transmission through families, which are caused by a single mutation in one of the following three genes: presenilin 1, presenilin 2, and amyloid precursor protein (APP). The genes encode the active site of γ-secretase, and the specific mutations increase the production of $A\beta_{42}$ leading to the early onset of familial AD.[2–4] In comparison, the sporadic form of AD is more complex and mainly results from a combination of genetic and environmental factors. Common symptoms of AD include memory loss, language abilities decline, orientation and cognitive skills destruction. The severity of these symptoms increases significantly with time. Neurofibrillary tangles and amyloid plaques are identified as the two pathological hallmarks of AD. Additionally, the loss of neurons and synapses has been observed in AD patient brains owing to the low level of the neurotransmitter acetylcholine.[5]

Several hypotheses have been proposed for a better understanding of the pathology of AD, including genetic causes, the cholinergic hypothesis, the amyloid cascade hypothesis, and the tau hypothesis. However, there exists no consensus on a generally accepted hypothesis. The amyloid cascade hypothesis provides a biochemical understanding of the pathological process, and speculates that the deposition of Aβ is the causative agent of the Alzheimer's pathology which results in tau hyperphosphorylation, axonal disruption, synapses loss, and ultimately cell death. The amyloidogenesis of Aβ in AD proceeds via conversion of dynamic ensembles of non-fibrillar and non-toxic conformers into β-sheet-rich cytotoxic assemblies. According to this hypothesis, several β- and γ-secretase inhibitors,[6,7] Aβ inhibitors[8–10] and anti-Aβ monoclonal antibodies[11,12] have been developed to achieve a balance between Aβ production and clearance. Aducanumab, the first disease-modifying AD therapeutic, preferentially binds to soluble Aβ oligomers and insoluble fibrils, while removing amyloid plaques in a dose- and time-dependent manner to slow or stop the progression of AD.[13] Although the amyloid cascade hypothesis allows to explain many pathogenic events, there are several concerns. The relationship between reduction of Aβ load and cognitive improvements is unclear. Most potential drugs can remove toxic aggregates, but the patient's memory function cannot be repaired, and the memory gap cannot be filled. Furthermore, the central nervous system is poorly penetrated by drugs which is a major barrier that limits the efficacy of these drugs in AD treatment. The human brain and AD pathogenesis is very complex. Therefore, only a comprehensive complication of all scientific evidence with respect to the clinical progression of AD can provide an understanding of the disease mechanism.

Aberrant amyloid aggregation is linked to the pathogenesis of several NDs, such as AD, amyotrophic lateral sclerosis (ALS), and Parkinson's disease (PD). It has been shown that these pathological amyloid aggregates co-localize with stress granules (SGs), and that interactions of amyloid proteins with SGs have consequences for the pathophysiology of diseases.[14,15] Additionally, maturation of SGs over time into insoluble aggregates contributes to disease.[16,17] In this review, we introduce first the relevance of SGs and LLPS in NDs with a focus on AD associated Aβ. Subsequently, we discuss the relationship between Aβ phase separation and aggregation, suggesting a potential pathway from Aβ phase transition to aggregation. Additionally, we review mechanistic aspects of Aβ aggregation kinetics focusing mainly on nucleation, fibril elongation, and heterogeneous nucleation processes. Finally, diverse polymorphic Aβ structural models are reviewed which might aid in structure-based drug design in diagnosis or treatment.

[a] *Dr. Z. Niu, S. Feng*
*School of Pharmacy, Henan University, Kaifeng, Henan 475004, China*
*E-mail: nz@henu.edu.cn*

[b] *Dr. X. Gui*
*Department of Structural Biology, St. Jude Children's Research Hospital, Memphis, TN, USA*

[c] *Prof. Dr. B. Reif*
*Bavarian NMR Center (B NMRZ), Department of Bioscience, TUM School of Natural Sciences, Technische Universität München (TUM), Garching 85747, Germany*
*E-mail: reif@tum.de*

[d] *Prof. Dr. B. Reif*
*Institute of Structural Biology (STB), Helmholtz-Zentrum München (HMGU), Neuherberg 85764, Germany.*

*© 2024 The Authors. Chemistry - A European Journal published by Wiley-VCH GmbH. This is an open access article under the terms of the Creative Commons Attribution Non-Commercial License, which permits use, distribution and reproduction in any medium, provided the original work is properly cited and is not used for commercial purposes.*

## 2. Stress Granules, Phase Separation and Amyloid Protein Aggregation

In recent years, LLPS-mediated aggregation has been proposed to be an important mechanism underlying the progression of several NDs.[14,18,19] The disease-associated proteins can undergo LLPS to form biomolecular condensates exhibiting liquid behavior, then mature into solid-like hydrogel over time via a liquid-to-solid phase transition (LSPT), and further aggregate into fibrillar aggregates. These pathogenic aggregates are related to SGs biology and play an important role in neurodegeneration. For example, AD-associated tau protein appears to regulate SGs formation and the interactions of tau protein with SGs have consequences for the pathophysiology of AD and tauopathies.[14] Microglial cells stressed by exposure to $A\beta_{42}$ peptides or fibrils form persistent SGs, leading to the production of reactive oxygen and nitrogen species that are toxic to neuronal cells.[20] SGs are dynamic cytoplasmic assemblies of mRNA and RNA-binding proteins (RBPs) formed via phase separation to help cell recovery from stress stimuli. They are transient structures that disperse when the environmental stress is removed. Low-complexity sequences and prion-like domains promote SG assembly. The subsequent disassembly and clearance of SGs are critical for restoration of normal cellular function.[21]

ALS is a neurodegenerative disease that primarily affects motor neurons in the brain and spinal cord. Evidence indicates that SGs are linked to ALS protein aggregation involved in the disease progression. The localization of superoxide dismutase 1 (SOD1), fused in sarcoma (FUS), and TAR DNA binding protein of 43 kDa (TDP-43) to SGs in cellular contexts of ALS patient suggests the facilitation role of SGs in ALS protein aggregation.[22–27] SGs may function as precursors in the formation of pathological aggregates. Mutant SOD1 increases the number of T cell-restricted intracellular antigen 1 (TIA-1) positive SGs and colocalizes with the SG marker Ras GTPase-activating protein binding protein 1 (G3BP1) in an RNA independent manner indicating the close link of SGs and neurodegeneration.[28,29] Additionally, ALS-mutations can perturb SG formation and alter its internal dynamics. Proteins associated with ALS promote the formation of SGs and the ALS-mutants enhance the accumulation of SGs in cells when exposed to stress conditions, thereby leading to SGs evolution and pathological aggregates formation. The chronic illness condition associated with aging, dysregulation of SGs, and mutations of SG components lead to chronic persistent SG formation. The persistent SGs function as seeds for protein aggregation that is associated with several NDs including ALS

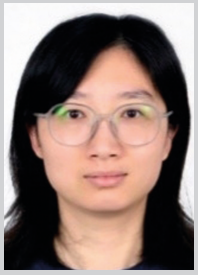

Dr. Zheng Niu is currently a principal investigator at Henan University. She obtained her doctoral degree in 2019 from Technische Universität München under the supervision of Prof. Dr. Bernd Reif. Her primary research interests lie in protein structure and function with a focus on elucidating the underlying mechanisms linking amyloid aberrant aggregation to neurodegeneration in neurodegenerative diseases such as Alzheimer's disease and Parkinson's disease.

Dr. Xinrui Gui got her Ph.D degree under the supervision of Prof. Dr. Cong Liu in cell biology in 2019. She focused on fibril structures of pathological amyloid proteins involved in ALS and frontotemporal dementia during pursuing her degree. She is now a postdoctoral fellow at St. Jude Children's research hospital with Prof. Dr. Tanja Mittag, where she continued her interests in understanding the interplay of phase separation and fibril formation of proteins involved in neurodegenerative diseases.

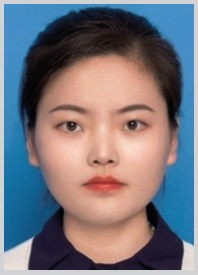

Shuang Feng obtained a Bachelor of Science degree from Huanghe University of Science and Technology in 2019, followed by a Master of Medicine degree from Henan University in 2023. During her graduate studies, she focused on the liquid-liquid phase separation and aberrant aggregation of amyloid peptide related to Alzheimer's disease.

Prof. Dr. Bernd Reif studied physics and biochemistry at the University Bayreuth. In 1998, he received his PhD in chemistry at the Goethe-University Frankfurt where he worked with Christian Griesinger. After a postdoctoral visit in the group of Robert G. Griffin at the Massachusetts Institute of Technology, Cambridge, USA, he was leading an Emmy-Noether research group of the DFG at the Technische Universität München. Between 2003 and 2010, Prof. Reif was was appointed at the Leibniz-Institut für Molekulare Pharmakologie (FMP) and at the Charité Universitätsmedizin Berlin. Since then, he is a professor for solid-state NMR at the Technische Universität München and the Helmholtz-Zentrum München. His research focuses on the development of MAS solid-state NMR methods for the characterization of structure and dynamics of proteins in the solid-state, as well as the application of solution- and solid-state NMR spectroscopy to the study of amyloidogenic peptides.


© 2024 The Authors. Chemistry - A European Journal published by Wiley-VCH GmbH

and PD.[23,30] The prominent pathological hallmark of PD is the deposition of α-synuclein (αS) in Lewy bodies. Recent research has shown that αS can undergo LLPS during its fibrillization. Over time, the maturation of the resulting condensates leads to a LSPT ultimately resulting in the amyloid deposition in cells.[18,31] Therefore, the fibrillar synuclein inclusions are formed via nucleation and elongation steps, or alternatively via LLPS and LSPT steps. These two distinct aggregation routes are linked to the pathogenesis and development of PD. Likewise, synuclein inclusions can localize in TIA-1 positive SGs suggesting the close interactions of SGs pathobiology and protein aggregation.[32]

Protein phase separation is a process that protein is spontaneously converted into a highly ordered state under certain conditions to achieve a dynamic equilibrium between the condensate phase and dilute phase. Defined low-complexity domains (LCDs) and intrinsically disordered regions allow various homotypic and heterotypic interactions of proteins with other biomolecules further drive LLPS.[33,34] Without defined LCDs, Aβ exhibits phase separation behavior due to its intrinsic disordered nature and inhomogeneous charge distribution. $Aβ_{42}$ globular oligomers ($Aβ_{42}$Os) can undergo LLPS to form liquid-like droplets via hydrophobic interactions in a membrane-mimicking environment of sodium dodecyl sulfate (SDS) under high kosmotropic salt conditions, promoting Aβ aggregation to form amyloid fibrils.[35] Amyloid oligomers as an important entity involved in protein LSPT and reveals the regulatory role of LLPS in amyloid protein oligomerization and aggregation, which may be relevant to the pathological process of AD. Targeting biomolecular condensates to block phase transition and protein aggregation offers new possibilities for drug development of AD.

Extensive evidence indicates that LLPS can either accelerate or suppress protein aggregation.[18,23,36] For example, the heterogeneous interactions of Aβ and ribosomal intergenic noncoding RNA facilitate the formation of nuclear amyloid bodies to regulate cell adaptation to stress stimuli. Upon stimuli termination, the heat-shock chaperone disaggregates amyloid bodies to mediate amyloidogenesis.[37] Further, the local environment of the condensed liquid may alter protein conformations thus disfavoring amyloid aggregation. The formation of liquid condensates induced by the heterotypic interactions and complex coacervation of $Aβ_{42}$ with DEAD-box proteins inhibits homotypic Aβ-Aβ interactions and further prevents amyloid aggregation.[38] However, the molecular mechanism of condensate-induced aggregation and the relationship between phase separation and amyloid aggregation have not been fully clarified. Different proteins require different amount of time to form a dense phase, indicating that biological phase separation is a nucleation-driven process rather than a spontaneous process.[39–42] Recent research suggests that the condensate-induced aggregation of αS within dense liquid condensates can be accelerated via the addition of αS fibril seeds through the secondary nucleation process.[43] LLPS may promote the nucleation and growth rate of protein assemblies in the condensed phase, transit into solid-like hydrogels or pathogenic amyloid fibrils composed of structurally ordered oligomers and fibrillar aggregates to further influence the aggregation kinetics, conformational dynamics, and molecular structures of amyloids.[44] As such, a comprehensive understanding of the structural basis and molecular mechanisms underlying amyloid protein condensation and aggregation pathway can facilitate a targeted therapeutic intervention against degenerative diseases.

Solution-state NMR has emerged as a powerful technique to analyze protein LLPS for detail structural information of the condensed phase. X-ray crystallography and cryo-EM are used for static structures determination, while solution-state NMR can characterize intermediates secondary/tertiary structures and transient molecular interactions further to obtain the structural details, protein motions, and conformational changes in a protein LLPS system.[45] With a combination of a probe molecule trifluoroethanol, the temporal and spatial measurement of protein LLPS can be characterized via $^{19}$F-detection NMR spectroscopy to deeply analyze the LLPS process and kinetics.[46] Furthermore, Eisenberg group have identified several segments from SG-associated protein LCDs that can form solid-like hydrogels and involved in membraneless assemblies.[47] They share a common kinked β-sheets structure termed as low-complexity aromatic-rich kinked segments (LARKS), which kinks at either glycine or aromatic residues. Within the β-sheets, the aromatic residues stabilize both intra- and inter- β-sheets. This kinked structure allows for lower buried surface areas and binding energies, which distinguished from the steric zipper structure identified in pathogenic amyloid fibrils. Additionally, by computational 3D profiling, they show LARKS are enriched in nucleoporins and ribonucleoproteins which are underlying the formation of phase-separated biomolecular condensates.

## 3. Aggregation of the Aβ Peptide in AD

Aβ is the cleavage product of β- and γ-secretases acting on APP in the amyloidogenic pathway (Figure 1). Imprecise cleavage by γ-secretase in the latter step results in several isoforms of Aβ peptide containing different C-terminuses, with the two major isoforms being $Aβ_{40}$ and $Aβ_{42}$. The underlying microscopic mechanism of Aβ aggregation consists of nucleation and elongation steps (Figure 1). The kinetic process of Aβ aggregation corresponds to a sigmoid growth pattern and is characterized by three phases: the lag phase, elongation phase, and saturation phase. During the initial lag phase, disordered soluble monomeric Aβ peptides accumulate to form nucleus. A rapid growth or elongation phase follows, wherein the monomer assembles into oligomers, protofibrils, and fibrils with distinct morphologies until the final saturation plateau phase. The fibrillar aggregates can be self-assembled via the primary nucleation pathway and elongated via monomer addition at the fibril end, and new species of oligomers or smaller aggregates can be formed via fibril fragmentation and surface-mediated secondary nucleation pathways.[48,49]

Secondary nucleation has emerged as a major pathway for new aggregates formation and may be responsible for the onset and progression of AD. *In vivo* studies suggest that the


© 2024 The Authors. Chemistry - A European Journal published by Wiley-VCH GmbH

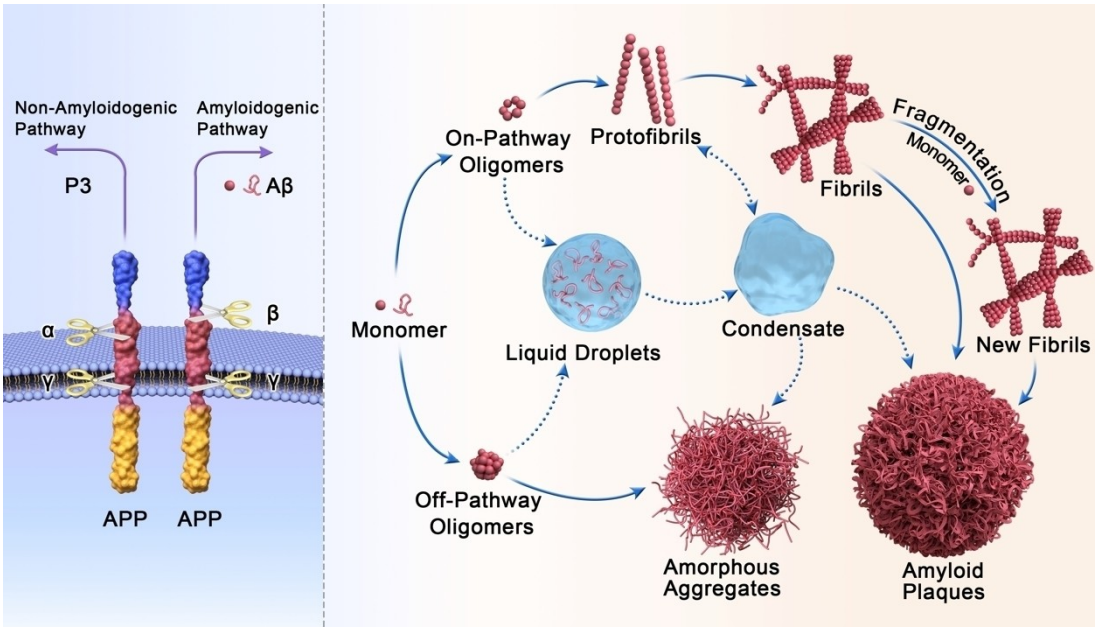


**Figure 1.** *The process of Aβ production and aggregation. Under amyloidogenic pathway, Aβ as a cleavage product is generated from APP. Monomeric disordered Aβ peptide aggregates into on-pathway oligomers, protofibrils and fibrils. Mature fibrils deposit into amyloid plaques. In off-pathway aggregation, monomeric disordered Aβ peptide assembles and deposits into amorphous aggregates. When the concentration and molecular weight threshold of Aβ oligomers is reached, the occurrence of phase separation is triggered by oligomers being recruited into liquid droplets, yielding biomolecular condensates. With the maturation of the condensates, protofibrils and mature fibrils can be formed. The prominent role of Aβ oligomerization in phase separation is key to understanding the potential correlation of these early events involved in the protein aggregation process, and can further explain the lack of an underlying mechanism of aberrant liquid-to-solid phase transition in the pathogenesis of AD.*

presence of existing amyloid fibrils at a given location in the brain can accelerate more fibrils formation ultimately leading to amyloid deposition spreading.[50,51] The novel non-invasive Drosophila models confirm the major role of secondary nucleation in amyloid formation and propagation of amyloid pathology throughout the brain, further reveal the direct linkage between seeded nucleation and neurotoxicity *in vivo*.[52] Under a low concentration of monomeric peptide, the aggregation process follows the primary nucleation pathway. When it reaches the critical concentration for amyloid fibril formation, sufficient surface for monomer attachment is formed inside the system. Consequently, the secondary nucleation pathway occurs via a fibril-catalyzed reaction, resulting in the formation of toxic oligomeric species (Figure 1). It should be noted that secondary nucleation may be a special case of surface nucleation[53] and can be detected through the systematic variation of monomer concentration in either unseeded or minimally seeded experiments.[54] When a high concentration of seeds is introduced into the aggregation system, the aggregation is dominated by fibril elongation, and the negligible contribution from secondary nucleation is difficult to estimate.[55] Several questions underlying the nucleation mechanism remain unanswered. Firstly, the formation location of the new aggregates in secondary nucleation needs to be identified, e.g., in a solution environment or at the fibril surface. Secondly, the reason why cross-catalysis of nucleation or a cross-seeding interaction occurs only in the primary nucleation pathway rather than the secondary nucleation pathway remains unclear. Thirdly, the driving force underlying these two nucleation processes is yet to be determined.

The transition of Aβ from the soluble monomeric state to the highly ordered aggregation state (Figure 1) depends on its intrinsic characteristics and the environmental conditions. Environmental conditions such as the incubation temperature, salt component, pH, and protein concentration result in different aggregation kinetics, which lead to structural and morphological diversity of Aβ amyloid strains. The fact that the molecular-level morphology can be transmitted by the seeding protocol indicates the conservation of the structural characteristics of Aβ fibril strains formed via fibril elongation, in which seeds function as a template to incorporate monomers at the ends of the existing fibrils and further to preserve the characteristics. However, there is limited evidence of the direct transmission of structural characteristics of amyloid strain via secondary nucleation. It has been shown that $A\beta_{42}$ can be cross-templated by $A\beta_{40}$ fibril ends, while $A\beta_{40}$ monomers are not efficiently incorporated into the end of $A\beta_{42}$ fibrils[56] indicating that the structural characteristics of fibrils formed through cross-surface nucleation were not defined by the seed structure, in contrast to fibril elongation. Additionally, seeding can efficiently accelerate Aβ aggregation owing to the low free energy barrier of fibril elongation via the addition of monomers at the fibril end in comparison with fibril formation from monomers via primary nucleation.[57,58] The saturation rate of fibril elongation is reached at a high monomer concentration, suggesting that the fibril elongation involves multiple steps. It probably involves an initial weak association between the


© 2024 The Authors. Chemistry - A European Journal published by Wiley-VCH GmbH

monomer and the seed fibril end, followed by a conformational search for the most thermodynamically stable state.[58]

In addition to the above nucleation process involved in Aβ aggregation, metal ions and lipid membranes induce heterogeneous nucleation process to regulate Aβ aggregation. Metal ions such as $Cu^{2+}$ and $Zn^{2+}$ bind directly to the N-terminal of Aβ monomeric peptide *in vitro*, mainly interact with the imidazole ring of histidine residues and the carboxyl group of glutamic acid residues, and maintain the β-sheet structure of the C-terminal hydrophobic region, forming amorphous aggregates.[59–61] Although it remains controversial whether the promotion or inhibition of $Cu^{2+}$ on Aβ aggregation kinetics, $Cu^{2+}$ binding redirects a conformational change while inducing neurotoxicity through the direct production of reactive oxygen species. $Cu^{2+}$ can bind with pre-formed $Aβ_{40}$ amyloid fibrils as well.[62] The morphology and conformational structure are retained upon addition of $Cu^{2+}$ to pre-formed $Aβ_{40}$ fibrils. However, the polymorphism of $Cu^{2+}$ coordination modes with pre-formed $Aβ_{40}$ fibrils were confirmed owing to various $Cu^{2+}$ binding sites.[63] Similarly, $Zn^{2+}$ binding with different morphologies of $Aβ_{42}$ oligomers results in different modes of coordination and significantly promotes Aβ aggregation by shortening the lag phase and reducing the solvation energy for $Zn^{2+}$-$Aβ_{42}$ oligomers.[60] The major species of these complexes exhibit a parallel β-sheet arrangement structure, and the polymorphisms including anti-parallel β-sheet arrangement and other less structured assemblies are stabilized owing to the presence of zinc ions. Because the conformational differences mainly depend on the different folding and misfolding pathways, such a polymorphism phenomenon can be attributed to the addition of metal ions to the Aβ aggregation process shifting the equilibrium of monomer, oligomers, and protofibrils, further modulating the thermodynamic kinetics by altering the energy landscape of Aβ aggregation.

Lipid or membrane surfaces, as typical nucleators, can modulate Aβ aggregation process. The negative surface of anionic lipid bilayers binding $Aβ_{40}$ peptide electrostatically leads to a structural conversion into β-sheet assemblies, and significantly accelerates the aggregation process by bypassing the lag phase.[64] The catalytic or template function can lower the energy barrier of the nucleation process and then mediate the aggregation pathway. In addition to the association on the membrane surface, Aβ can firmly anchor into membranes resulting in the formation of ion channel-like pores.[65] Aβ oligomers directly interact with membranes and the resulting pore-like structures leads to the membrane permeability disruption. A two-step scenario has been proposed to describe the membrane disruptions in the presence of gangliosides-clusters.[66] At the beginning, Aβ oligomers bind to the membrane resulting in a pore-like channel formation. Thereafter, Aβ self-assembles into fibrils during the elongation and saturation phase induced membrane disruption and fragmentation in a detergent-like manner. Consequently, Aβ-lipid/membrane interactions[67–69] with different assembly species exert different cytotoxicity relevant to AD. Annular protofibril formed from pore-structured oligomer is responsible to ion dysregulation. Additionally, Aβ oligomeric aggregates generated by the secondary nucleation process have been reported to exhibit a dominant role in the disruption of membrane both *in vitro* and *in vivo*, and consequently influence the homeostasis of $Ca^{2+}$ resulting in neurotoxicity.[70] Although Aβ aggregation kinetics *in vitro* have been extensively studied, the molecular mechanism of protein aggregation in AD patients' brain or lipid membrane and the connections between Aβ pathological aggregation and lipid bilayer permeability are poorly understood. Further investigation into the underlying mechanism of toxicity of various Aβ species will provide potential therapeutic targets for AD treatment.

Protein aggregation can be categorized as a sequential oligomerization process. The resulting oligomers have important functions and exert neurotoxicity, which is highly relevant to NDs. Oligomerization has been reported to be closely linked to protein LLPS. For example, the oligomerization of the globular N-terminal domain facilitates the LLPS of full-length TDP-43.[71] Phase separation of $Aβ_{42}$ globulomer contributes to fibrillar aggregation.[35] Additionally, oligomerization has been proposed as a potential mechanism for organizing and concentrating functional components within membraneless cellular bodies. High-order oligomerization of speckle-type POZ protein (SPOP) promotes localization to nuclear speckles and stimulate the substrate ubiquitination.[72] Likewise, nanoclusters formed via αS high-order oligomerization in bulk solution have been demonstrated to undergo LLPS, further accelerating αS aggregation in the dilute phase over time.[31] Oligomerization typically precedes and contributes to protein LLPS, thereby promoting the formation of SGs. The accumulation of toxic oligomers is highly relevant to the pathogenesis of NDs. Better understanding of the relationship between oligomerization, phase separation and SGs biology will provide deeper insights into the pathogenesis and progression of NDs and pave the way for the development of novel therapeutic strategies aimed at preventing or reversing protein aggregation-related neuropathology.

## 4. Structural Polymorphism

Structural polymorphism indicates the structural variations of amyloid aggregates at the molecular level both *in vitro* and *in vivo.* Owing to the complex aggregation process, amyloid polymorphism and structural heterogeneity have been reported in many misfolding protein systems, such as Aβ,[73,74] αS,[75,76] and islet amyloid polypeptide (IAPP).[77,78] Here, we focus on the polymorphism phenomenon of Aβ species.

### 4.1. Aβ Segments and Oligomers

The first Aβ segment structures were determined by Eisenberg group.[79] Segments $^{37}$GGVVIA$^{42}$ and $^{35}$MVGGVV$^{40}$ from the C-terminus of Aβ exhibit a structure termed as steric zipper, which is composed of two tightly mating repetitive cross-β sheets with the hydrogen bonds formed by the backbone amino groups within β-sheet layers and the van der Waals forces of


© 2024 The Authors. Chemistry - A European Journal published by Wiley-VCH GmbH

the dry integrating interface render the main forces that stabilizing amyloid fibrils. The steric zipper structures can be categorized into different classes distinguished by whether their sheets are parallel or anti-parallel, packing with the same or different surfaces, in or out of register. As such, one identical segment of Aβ can form distinct types of steric zipper structures. For example, segment $^{16}$KLVFFA$^{21}$ displays three crystal forms, differ in conformations of Lys16 and Phe20. Segment $^{27}$NKGAII$^{32}$ forms parallel β-sheet structures with different steric zipper interfaces.[80] The packing polymorphism may reveal the fundamental information of amyloid polymorphism.

The crystalized segments of Aβ are typically containing 4~10 amino acid residues in length. Longer segments tend to grow smaller crystals that is challenged for structural determination by X-ray diffraction.[81,82] However, with the development of micro-electron diffraction (microED) which is ideally suitable for nano-sized crystals, the structures of longer segments of Aβ ($Aβ_{24-34}$, D23N-$Aβ_{16-26}$ and $Aβ_{20-34}$) have been determined, showing similarities with shorter peptides and full-length Aβ structures.[9,83,84] Although the structures of short segments can undoubtedly reveal the molecular basis for amyloid structure and stability at the atomic level, they can only offer limited information about full amyloid fibrils. Furthermore, the segments show generally homo-steric zippers structures whereas the hetero-steric zippers are more often reported in the full-length amyloid fibrils determined by NMR and cryo-EM.[85]

Aβ oligomers vary widely with regard to size and morphology, which introduces significant obstacles to obtaining the structural information at the atomic level because of the highly dynamic nature. Although challenged, a low-temperature and low-salt preparation approach was established to capture pentamers and decamers of $Aβ_{42}$.[86] The disc-shaped on-pathway oligomers have been observed with average widths of 10–15 nm and heights of 2–4 nm. Instead of the β-sheet secondary structure, this type of oligomer exhibits loose strands and is more toxic than mature $Aβ_{42}$ fibrils. Additionally, the interactions between hydrophobic residues in the C-terminus of $Aβ_{42}$ and hydrophobic chains of SDS can reconfigure $Aβ_{42}$ oligomers, which leads to the formation of liquid-like droplets,[35] indicating that the structures of Aβ oligomers may be involved in SG formation and LLPS. In contrast to the on-pathway oligomers, a spherical off-pathway amyloid assembly of $Aβ_{42}$ has been reported containing a β-loop-β motif and exhibiting a unique off-register parallel β-sheet alignment.[87] The distinct differences of secondary and tertiary structures suggest that the β-sheet alignment and rearrangement result in both conformation and kinetic regime changes of different types of $Aβ_{42}$ oligomers.

$PrP^C$, as one of the cell-surface receptors for Aβ, has been exploited to sequester Aβ oligomers through coprecipitating.[88–90] In a complex of $Aβ_{42}$ oligomers and $PrP^C$, high-molecular weight Aβ heteroassemblies adopt a β-strand-rich conformation and exhibit reduced toxic effects in a concentration-dependent manner upon the addition of either N-terminal or full-length human $PrP^C$.[90] Moreover, $PrP^C$ slowed Aβ fibrils formation by selectively binding to the rapid growing end of each fibril, thus specifically inhibiting the elongation of Aβ fibrils.[89] Instead of binding to $PrP^C$, fusing $Aβ_{42}$ to the soluble domain of the α-hemolysin (αHL) toxin was considered as an alternative to stabilize $Aβ_{42}$ oligomers in the membrane environment.[91] The atomic level structure of the complex $Aβ_{42}$-αHL oligomers was determined by using cryo-EM with an overall resolution of 3.3 Å, and they exhibited similarities to wild-type $Aβ_{42}$ pore oligomers with regard to their structure, function, and biological properties (PDB ID: 7O1Q).

The first three-dimensional structure of pore-forming $Aβ_{42}$ tetramers formed in a membrane mimicking environment was reported by Ciudad et al.[92] The β-sheet pore-forming $Aβ_{42}$ oligomers were incorporated into the micelles of dodecylphosphocholine and harbored a six stranded tetramer unit exhibiting pore-like behavior (PDB ID: 6RHY). With an increase in the peptide concentration, $Aβ_{42}$ octamers emerged as well, which were formed by two tetramers facing each other in a β-sandwich structure. In addition to structural characterization *in vitro*, brain derived Aβ oligomers linked to different nucleation pathways were classified and distinguished by conformation-specific antibodies.[93] The oligomers which are mainly formed by the primary nucleation process have no spatiotemporal relationship with amyloid plaques. Therefore, they do not contain the structural features of amyloid fibrils and have an out-of-register architecture. In contrast, another type of oligomers which are formed by the secondary nucleation process appear after amyloid plaques, and are catalyzed by pre-formed Aβ fibrils. They share a common quaternary structure with Aβ fibrils and adopt an in-register β-sheets architecture.

### 4.2. $Aβ_{40}$ Fibrils

Fibrils, which result from misregulation or insufficient degradation due to aging, have been extensively studied owing to their significant role in neurotoxicity in the pathological characteristics of AD. With regard to $Aβ_{40}$ fibrils, there are two typical morphologies induced by different fibrils growth conditions *in vitro:* the striated ribbon morphology and twisted morphology.[94] They are arranged in a parallel β-sheet in-register array and share a common secondary and tertiary structure, rather than quaternary structure and overall symmetry of fibrils. The striated ribbon fibrils have two-fold rotational symmetry (PDB ID: 2LMN, 2LMO; structural details are presented in Table 1, and structural models of chain A are shown in Figure 2a–b), whereas the twisted fibrils exhibit three-fold symmetry (PDB ID: 2LMP, 2LMQ; structural details are presented in Table 1, and structural models of chain A are shown in Figure 2c–d). Furthermore, the salt bridge formed by the side chains of Asp23 and Lys28, which stabilizes the fibrils' structure, is only present in the striated ribbon fibrils. In addition, the racemic mixtures of $Aβ_{40}$ fibrils ($_{D,L}$-$Aβ_{40}$ fibrils) exhibit a qualitatively different supramolecular structure, that is, antiparallel "rippled sheet" structures.[95] The structural differences may arise from different side-chain packing arrangements and side chain-side chain interactions, which alter hydrogen-bond registries ultimately leading to amyloid polymorphism.

The Iowa-mutant D23N-$Aβ_{40}$ fibrils have either the parallel[96] or antiparallel[97] architecture of the backbone conformations.


© 2024 The Authors. Chemistry - A European Journal published by Wiley-VCH GmbH

**Table 1.** Atomic resolution structural details indicating amyloid polymorphism.

| Peptide | Source | Method | Characteristic | PDB ID |
|---|---|---|---|---|
| $A\beta_{40}$ | recombinant peptide | SSNMR | In-register parallel β-sheets structure with twisted morphology (3-fold symmetry) and striated ribbon morphology (2-fold symmetry). | 2LMN, 2LMO, 2LMP, 2LMQ |
| $A\beta_{40}$ | seeded from brain tissue | SSNMR | Twisted morphology contains 3 cross-β units. A twist structure in residues 19–23, a kink at G33 and a bend at residues 37–38. | 2M4J |
| $A\beta_{40}$ | extracted from meningeal tissue | cryo-EM | Right-hand twisted morphology and consists of two stacks of peptide. Each peptide contains 4 β stands. | 6SHS |
| $A\beta_{40}$ | seeded with fibrils extracted from cortical tissue | cryo-EM | Four layers in inner cross-β units, and β-hairpins in outer cross-β units. | 6W0O |
| $A\beta_{40}$ D23N | synthetic peptide | SSNMR | In-register, parallel β-sheet model | 2MPZ |
| $A\beta_{40}$ D23N | recombinant peptide | SSNMR | Double-layered antiparallel β-sheet model | 2LNQ |
| $A\beta_{40}$ E22Δ | recombinant peptide | SSNMR | In-register, parallel architecture containing 5 β stands. | 2MVX |
| $A\beta_{40}$ and $A\beta_{42}$ co-fibril | recombinant peptide | SSNMR | U-shape β1-turn-β2 structure and packed into a parallel in-registry β-spine. | 6TI6 |
| $A\beta_{42}$ | recombinant peptide | SSNMR | In-register, parallel β-sheets architecture with β-strand-turn-β-strand shape conformation | 2BEG |
| $A\beta_{42}$ | recombinant peptide | SSNMR | S-shaped triple parallel-β-sheet conformation. | 2MXU |
| $A\beta_{42}$ | recombinant peptide | SSNMR | Two molecules per fibril layer, containing four β-strands in a S-shaped conformation. | 5KK3 |
| $A\beta_{42}$ | recombinant peptide | SSNMR | Two molecules per fibril layer, forming a double-horseshoe-like cross-β-sheet conformation. | 2NAO |
| $A\beta_{42}$ | recombinant peptide | cryo-EM | Two molecules per fibril layer forming cross-β structure with face-to-face packing, and the C-termini locating at the dimer interface. | 5AEF |
| $A\beta_{42}$ | recombinant peptide | cryo-EM | Two molecules per fibril layer with L-shaped N-terminus and S-shaped C terminus. | 5OQV |
| $A\beta_{42}$ | Extracted from the brain of a patient with AD, type I filaments | cryo-EM | Left-handed twisted filaments extend from Gly9 to Ala42 containing two identical S-shaped protofilaments including two hydrophobic clusters with 5 β stands. | 7Q4B |
| $A\beta_{42}$ | Extracted from the brain of a patient with AD, type II filaments | cryo-EM | Left-handed twisted filaments extend from Val12 to Ala42 containing two identical S-shaped protofilaments including two hydrophobic clusters with 4 β stands. | 7Q4M |

Parallel Iowa-mutant D23N-$A\beta_{40}$ fibrils (PDB ID: 2MPZ; structural details are presented in Table 1, shown in Figure 3a) contain less extended hydrophobic core than wide-type $A\beta_{40}$ fibrils, and more extended hydrophobic core than antiparallel Iowa-mutant D23N-$A\beta_{40}$ fibrils (PDB ID: 2LNQ; structural details are presented in Table 1, shown in Figure 3c). The polymorphs of familial mutated $A\beta_{40}$ fibrils are linked to the phenotypic diversity. The overall structural model of Osaka mutation E22Δ-$A\beta_{40}$ fibrils (PDB ID: 2MVX; structural details are presented in Table 1, shown in Figure 3b) is arranged in a parallel in-register architecture with a single morphology and two-fold symmetry arrangement.[98] Moreover, Aβ fibrils may propagate their molecular architectures and polymorphism in AD patients' brains, and this amyloid polymorphism *in vivo* may correlate with the progression of AD. The first atomic level structure of brain tissue derived $A\beta_{40}$ fibrils exhibited a specific morphism and an irregular secondary structure including a twist in residues Phe19-Asp23, a kink at residue Gly33, and a bend in residues Gly37 and Gly38 (PDB ID: 2M4J; structural details are presented in Table 1, shown in Figure 3d),[99] which is similar to the fibrils formed in a lipid vesicle environment.[64] Additionally, one single predominant $A\beta_{40}$ fibril structure can be determined from patients' brain occipital lobe tissue, frontal lobe tissue, and temporal lobe tissue,[100] which is nearly identical to $A\beta_{40}$ fibrils prepared *in vitro* exhibiting a three-fold symmetry along the


© 2024 The Authors. Chemistry - A European Journal published by Wiley-VCH GmbH

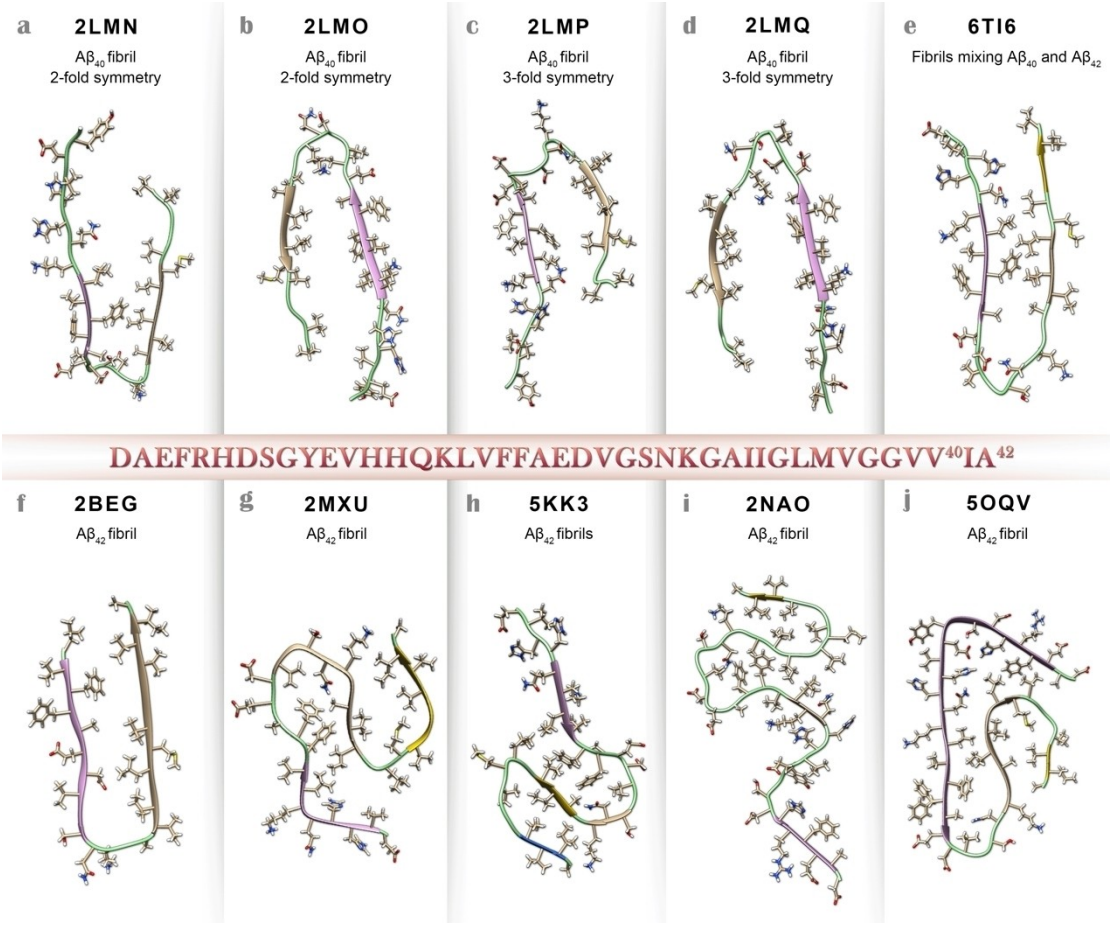


**Figure 2.** *Structural models of Aβ fibrils show the amyloid polymorphism. Every PDB structure is represented by chain A. a–b): structural models of $A\beta_{40}$ fibrils with two-fold symmetry; c–d): structural models of $A\beta_{40}$ fibrils with three-fold symmetry; e): a new structural model by mixing $A\beta_{40}$ and $A\beta_{42}$ peptides; f): 3D structure of $A\beta_{42}$ fibrils; g–i): atomic resolution structures of $A\beta_{42}$ fibrils are determined by solid-state NMR; j) near-atomic resolution fibril structure of complete $A\beta_{42}$ by cryo-EM. PDB structures are plotted by UCSF Chimera.*[113]

fibril axis and coexisting with structurally ordered and disordered segments.

Benefitting from the technological development of electron microscopes, detectors, and image processing software, cryo-EM has become a powerful technique for investigating challenging macromolecular complex systems and for protein structural characterization. Significant advancements have been made in the determination of protein structures in the last two decades. The molecular structure and morphology of $A\beta_{40}$ fibrils from both meningeal and cortical AD patient's brain have been characterized using cryo-EM (PDB ID: 6SHS, 6 W0O; structural details are presented in Table 1, shown in Figure 3e–f).[101,102] The meningeal tissue derived Aβ fibrils of patients (PDB ID: 6SHS) are polymorphic, and one observed morphology is the right-handed twisted β-sheet. Instead of the disordered N-terminus of *in vitro* $A\beta_{40}$ fibril models, the N-terminal segment formed a β-sheet structure in brain tissue. Each layer of Aβ fibrils extracted from brain tissue contained two stacked peptides, and each peptide contained four β-sheet structures.

### 4.3. $A\beta_{42}$ Fibrils

Owing to the different propensity for misfolding and self-assembly, the conformational heterogeneity has been identified of $A\beta_{42}$ fibrils compared with $A\beta_{40}$ fibrils. Different architecture packing including β-strands organization and monomer unit configuration can be attributed to their different primary structures and distinct aggregation kinetics. Monomer units can be arranged in either a two-fold or a three-fold symmetry in $A\beta_{40}$ fibrils, whereas only a two-fold symmetry configuration is observed in $A\beta_{42}$ fibrils. Two additional amino acids at the C-terminal of $A\beta_{42}$ promotes the formation of a longer hydrophobic cluster during its aggregation leading to different structures of the rigid fibril core compared with $A\beta_{40}$ fibrils. In addition, different sequences of the dynamic regions lead to different conformations on the fibrils surface which potentially result in different functional activities of amyloid fibrils.

*In vitro* structural models of $A\beta_{42}$ fibrils determined via solid-state NMR are highly homogenous, have similar structural features, and exhibit only one morphology with the S-shaped β-sheet arrangement shown in Figure 4c–e (PDB ID: 2MXU, 2NAO, 5KK3).[103–105] The molecules are arranged in a parallel in-register


© 2024 The Authors. Chemistry - A European Journal published by Wiley-VCH GmbH

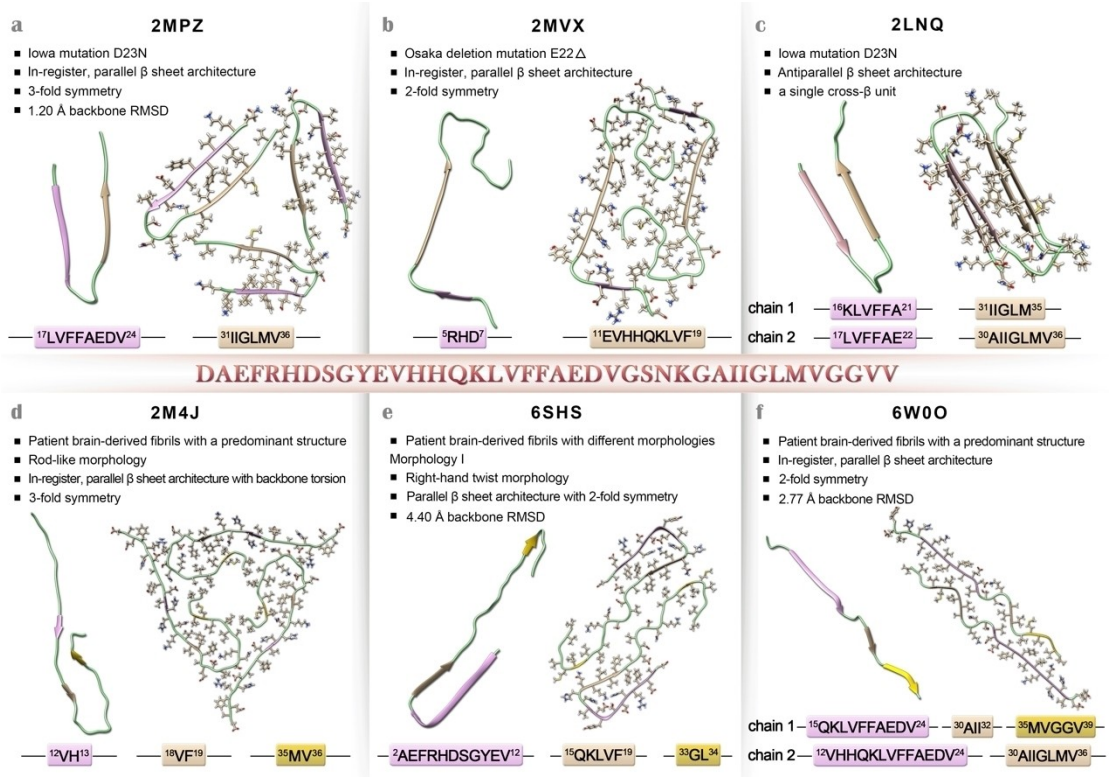


**Figure 3.** *Molecular structural models of $A\beta_{40}$ fibrils. a): Iowa-mutant D23N-$A\beta_{40}$ fibrils, PDB ID: 2MPZ; b): Osaka deletion mutation E22Δ-$A\beta_{40}$ fibrils, PDB ID: 2MVX; c): Iowa-mutant D23N-$A\beta_{40}$ fibrils, PDB ID: 2LNQ; d-f): brain tissue derived $A\beta_{40}$ fibrils determined by solid-state NMR (d, PDB ID: 2M4J) or cryo-EM (e and f, PDB ID: 6SHS and 6W0O). PDB structures are plotted by UCSF Chimera.*[113]

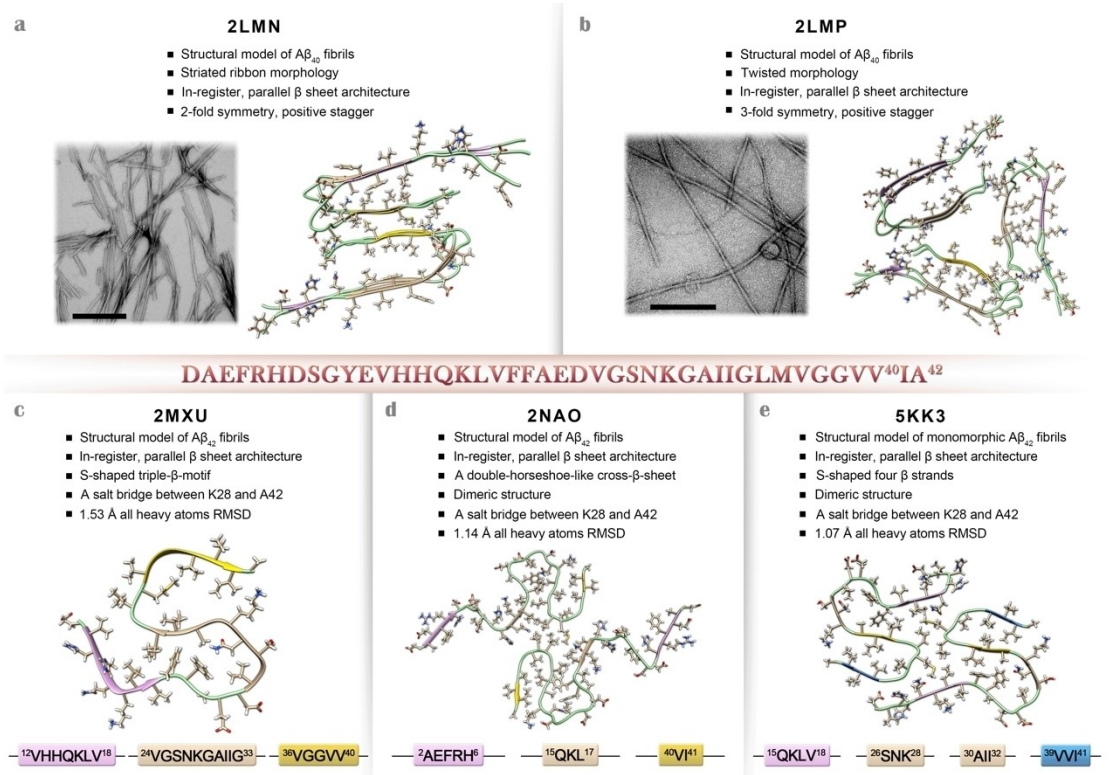


**Figure 4.** *Structural models for Aβ fibrils determined by using solid-state NMR. a): structural model of $A\beta_{40}$ fibrils with two-fold symmetry, PDB ID: 2LMN; b): structural model of $A\beta_{40}$ fibrils with three-fold symmetry, PDB ID: 2LMP; c): structural model of $A\beta_{42}$ fibrils, PDB ID: 2MXU; d): structural model of a disease relevant $A\beta_{42}$ fibrils, PDB ID: 2NAO; e): Structure model of monomorphic $A\beta_{42}$ fibrils, PDB ID: 5KK3. PDB structures are plotted by UCSF Chimera.*[113] *The TEM images are adapted by the permission of Elsevier and scale bars represent 200 nm.*[73] *Copyright 2015 Elsevier Inc.*


© 2024 The Authors. Chemistry - A European Journal published by Wiley-VCH GmbH

array, and two $A\beta_{42}$ molecules are in contact via inter-molecular interactions on the different molecules in each fibril layer (structural details are presented in Table 1, and structural models of chain A are shown in Figure 2g–i). Recently, a novel fold structure of brain derived $A\beta_{42}$ fibrils has been determined via sensitivity-enhanced proton detection NMR.[106] The structure with a less twisted morphology contains a triple-β motif and exhibits different β-strand locations from the above S-shaped structure, indicating that multiple forms of $A\beta_{42}$ fibrils *in vitro*.

In addition to the above structures determined via solid-state NMR, the structural determination of $A\beta_{42}$ fibrils has been achieved using cryo-EM. Synthetic $A\beta_{42}$ peptides were incubated to prepare fibrils in an aqueous solution with a pH of 7.4 (PDB ID: 5AEF).[107] Compared with the model of dimeric $A\beta_{40}$ fibrils, $A\beta_{42}$ dimeric peptides have identical tilde-shaped conformations and same pattern of interactions through hydrophobic C-terminal β-strands. The C-terminal segment of $A\beta_{42}$ fibrils forms the fibrillar core and is located at the dimer interface, which is surrounded by the N-terminus. The low intensity of the N-terminus indicates that it is flexible and dynamic, which is suitable for antibody binding. With a combination of cryo-EM and solid-state NMR, the molecular structure of recombinant $A\beta_{42}$ fibrils were determined and comprised two inter-wined protofilaments with 4 Å resolution (PDB ID: 5OQV).[108] The β-strand segments were organized into a parallel in-register array, similar to the solid-state NMR structure presented above. However, the difference is that the peripheral β-sheets were tilted by ~10° with respect to the growth axis of fibrils. In addition, the dimer interface and the turn region of residue Phe20 to residue Gly25 exhibited considerable differences compared with the NMR structure.

Recently, cryo-EM structures of $A\beta_{42}$ filaments derived from sporadic AD patients were reported and mainly exhibited a left-handed twisted morphology (type I morphology, PDB ID: 7Q4B) with two identical S-shaped protofilaments containing two hydrophobic clusters. Type I filaments extend from Gly9 to Val42 and contain five β-strands. Another twist morphology of filaments (type II morphology, PDB ID: 7Q4M) was observed in familial AD and other conditions.[109] It exhibits similar S-shaped protofilaments and the same side chain orientations. Compared with type I filaments, the main differences are the orientations of residues, including Gly25 to Ser26 and Val36 to Gly37, resulting in the expansion of the hydrophobic clusters. The above two morphologies differ significantly from those of the $A\beta_{42}$ fibrils formed *in vitro*; however, the type I morphology is similar to the molecular structure of the Osaka deletion mutation. As indicated by recent research results, a unique amyloid fibril is produced by mixing of $A\beta_{40}$ and $A\beta_{42}$ peptides since there exist cross-interactions between $A\beta_{40}$ and $A\beta_{42}$ *in vivo*. The novel interlaced fibril structure is distinct from each pure fibrils adopting a U-shaped β1-turn-β2 structure register with the requirements of both $A\beta_{40}$ and $A\beta_{42}$ filaments (PDB ID: 6TI6; structural models of chain A are shown in Figure 2e).[110]

As such, amyloid polymorphism raises the challenges for structural determination, molecular imaging, and therapy. The most suitable methods to distinguish these pathogenic amyloid oligomers and fibrils with different morphologies and how these polymorphisms are linked to the progression of diseases remain unclear. Gold nanoparticles (NPs) were developed as an efficient tool for direct characterization of amyloid polymorphism under hydrated conditions. These NPs with a core diameter of 3 nm can be used to label the edges of synthetic, recombinant, and tissue-derived amyloid fibrils.[111] The labeling scheme improves visualization under cryo-EM, which is helpful for studying the polymorphic distribution. In addition, quantitative image analysis such as the width and length of amyloid aggregate measurements, can be performed using gold NP decoration. Owing to the significance of distinguishing or targeting the polymorphs, researchers have found that the environmental or hydrodynamic stress in solution can modulate or control amyloid polymorphism.[112] According to their results, only a homogeneous rod-like amyloid morphology can be screened under high-stress conditions. Compared with high-stress environments, low-stress conditions generate heterogeneous amyloid fibrils containing twisted, helical, and rod-like morphologies. Future anti-Aβ drug design should focus on the modulation of amyloidogenicity and further to target different Aβ species with polymorphism via conformational control during the aggregation process.

## 5. Conclusions and Outlook

Protein misfolding and aberrant aggregation are linked to the loss of protein function, cell degeneration, and the pathogenesis of NDs. This review introduces the microscopic mechanism of Aβ aggregation with a focus on the nucleation and fibril elongation, discusses the relationship between SGs formation, LLPS, and amyloid protein aggregation, and summarizes the latest molecular Aβ fibril structures which will be important in the future to enable structure-based drug design. The failure of anti-Aβ therapy has been partly attributed to the late intervention in the disease process. To delay the onset of more severe symptoms, early intervention in treatment of the disease is needed. Furthermore, AD associated symptoms and pathology have to be distinguished from other dementias to make medications more effective in particular during early stages. The search and identification of selective, early stage inhibitors that suppress either primary or secondary nucleation processes is thus an important milestone to reach this goal. In addition, strategies involving SG formation in ND treatment have been developed. In these strategies, the scaffold is targeted either directly or indirectly by addressing clients of the phase-separated compartment, such as chaperones, which allows to modulate the biophysical properties of the SGs. Decoding the structural mechanism of inhibition of aggregation, elucidating the molecular recognition of Aβ deposits or understanding the process of clearance of toxic species will aid the development of strategies for AD diagnosis and treatment. The identification of such essential aspects will be crucial for gaining mechanistic insights into AD pathogenesis and developing novel diagnostics and therapeutics.


© 2024 The Authors. Chemistry - A European Journal published by Wiley-VCH GmbH

## Acknowledgements

This work was supported by the National Natural Science Foundation of China (Grant No. 32100964) and the German Science Foundation (project Re1435). We acknowledge support from the Helmholtz-Gemeinschaft and the Bavarian NMR Center (http://www.bnmrz.org). Open Access funding enabled and organized by Projekt DEAL.

## Conflict of Interests

There are no conflicts to declare.

## Data Availability Statement

Data sharing is not applicable to this article as no new data were created or analyzed in this study.

**Keywords:** Alzheimer's disease · amyloid-β peptide · protein aggregation · liquid-liquid phase separation · solid-state NMR

[1] Alzheimer's Association, *Alzheimer's Dementia* **2019**, *15*, 321–387.
[2] D. S. Knopman, H. Amieva, R. C. Petersen, G. Chételat, D. M. Holtzman, B. T. Hyman, R. A. Nixon, D. T. Jones, *Nat. Rev. Dis. Primer* **2021**, *7*, 33.
[3] Y.-F. Shea, L.-W. Chu, A. O.-K. Chan, J. Ha, Y. Li, Y.-Q. Song, *J. Formosan Med. Assoc.* **2016**, *115*, 67–75.
[4] H. Zetterberg, N. Mattsson, *Expert Rev. Neurother.* **2014**, *14*, 621–630.
[5] D. J. Selkoe, *Science* **2002**, *298*, 789–791.
[6] H. F. Dovey, V. John, J. P. Anderson, L. Z. Chen, P. De Saint Andrieu, L. Y. Fang, S. B. Freedman, B. Folmer, E. Goldbach, E. J. Holsztynska, K. L. Hu, K. L. Johnson-Wood, S. L. Kennedy, D. Kholodenko, J. E. Knops, L. H. Latimer, M. Lee, Z. Liao, I. M. Lieberburg, R. N. Motter, L. C. Mutter, J. Nietz, K. P. Quinn, K. L. Sacchi, P. A. Seubert, G. M. Shopp, E. D. Thorsett, J. S. Tung, J. Wu, S. Yang, C. T. Yin, D. B. Schenk, P. C. May, L. D. Altstiel, M. H. Bender, L. N. Boggs, T. C. Britton, J. C. Clemens, D. L. Czilli, D. K. Dieckman-McGinty, J. J. Droste, K. S. Fuson, B. D. Gitter, P. A. Hyslop, E. M. Johnstone, W.-Y. Li, S. P. Little, T. E. Mabry, F. D. Miller, B. Ni, J. S. Nissen, W. J. Porter, B. D. Potts, J. K. Reel, D. Stephenson, Y. Su, L. A. Shipley, C. A. Whitesitt, T. Yin, J. E. Audia, *J. Neurochem.* **2009**, *76*, 173–181.
[7] N. M. Moussa-Pacha, S. M. Abdin, H. A. Omar, H. Alniss, T. H. Al-Tel, *Med. Res. Rev.* **2020**, *40*, 339–384.
[8] Z. Najarzadeh, H. Mohammad-Beigi, J. Nedergaard Pedersen, G. Christiansen, T. V. Sønderby, S. A. Shojaosadati, D. Morshedi, K. Strømgaard, G. Meisl, D. Sutherland, J. Skov Pedersen, D. E. Otzen, *Biomol. Eng.* **2019**, *9*, 659.
[9] S. L. Griner, P. Seidler, J. Bowler, K. A. Murray, T. P. Yang, S. Sahay, M. R. Sawaya, D. Cascio, J. A. Rodriguez, S. Philipp, J. Sosna, C. G. Glabe, T. Gonen, D. S. Eisenberg, *eLife* **2019**, *8*, e46924.
[10] K. Wiesehan, K. Buder, R. P. Linke, S. Patt, M. Stoldt, E. Unger, B. Schmitt, E. Bucci, D. Willbold, *ChemBioChem* **2003**, *4*, 748–753.
[11] R. S. Doody, R. G. Thomas, M. Farlow, T. Iwatsubo, B. Vellas, S. Joffe, K. Kieburtz, R. Raman, X. Sun, P. S. Aisen, E. Siemers, H. Liu-Seifert, R. Mohs, *N. Engl. J. Med.* **2014**, *370*, 311–321.
[12] C. H. van Dyck, *Biol. Psychiatry* **2018**, *83*, 311–319.
[13] J. Sevigny, P. Chiao, T. Bussière, P. H. Weinreb, L. Williams, M. Maier, R. Dunstan, S. Salloway, T. Chen, Y. Ling, J. O'Gorman, F. Qian, M. Arastu, M. Li, S. Chollate, M. S. Brennan, O. Quintero-Monzon, R. H. Scannevin, H. M. Arnold, T. Engber, K. Rhodes, J. Ferrero, Y. Hang, A. Mikulskis, J. Grimm, C. Hock, R. M. Nitsch, A. Sandrock, *Nature* **2016**, *537*, 50–56.
[14] S. Wegmann, B. Eftekharzadeh, K. Tepper, K. M. Zoltowska, R. E. Bennett, S. Dujardin, P. R. Laskowski, D. MacKenzie, T. Kamath, C. Commins, C. Vanderburg, A. D. Roe, Z. Fan, A. M. Molliex, A. Hernandez-Vega, D. Muller, A. A. Hyman, E. Mandelkow, J. P. Taylor, B. T. Hyman, *EMBO J.* **2018**, *37*, e98049.
[15] E. Hallacli, C. Kayatekin, S. Nazeen, X. H. Wang, Z. Sheinkopf, S. Sathyakumar, S. Sarkar, X. Jiang, X. Dong, R. Di Maio, W. Wang, M. T. Keeney, D. Felsky, J. Sandoe, A. Vahdatshoar, N. D. Udeshi, D. R. Mani, S. A. Carr, S. Lindquist, P. L. De Jager, D. P. Bartel, C. L. Myers, J. T. Greenamyre, M. B. Feany, S. R. Sunyaev, C. Y. Chung, V. Khurana, *Cell* **2022**, *185*, 2035–2056.e33.
[16] J. L. Martin, S. J. Dawson, J. E. Gale, *Hear. Res.* **2022**, *426*, 108634.
[17] B. Wolozin, P. Ivanov, *Nat. Rev. Neurosci.* **2019**, *20*, 649–666.
[18] S. Ray, N. Singh, R. Kumar, K. Patel, S. Pandey, D. Datta, J. Mahato, R. Panigrahi, A. Navalkar, S. Mehra, L. Gadhe, D. Chatterjee, A. S. Sawner, S. Maiti, S. Bhatia, J. A. Gerez, A. Chowdhury, A. Kumar, R. Padinhateeri, R. Riek, G. Krishnamoorthy, S. K. Maji, *Nat. Chem.* **2020**, *12*, 705–716.
[19] L. Pytowski, C. F. Lee, A. C. Foley, D. J. Vaux, L. Jean, *Proc. Nat. Acad. Sci.* **2020**, *117*, 12050–12061.
[20] S. Ghosh, R. L. Geahlen, *EBioMedicine* **2015**, *2*, 1785–1798.
[21] D. S. W. Protter, R. Parker, *Trends Cell Biol.* **2016**, *26*, 668–679.
[22] N. Samanta, S. S. Ribeiro, M. Becker, E. Laborie, R. Pollak, S. Timr, F. Sterpone, S. Ebbinghaus, *J. Am. Chem. Soc.* **2021**, *143*, 19909–19918.
[23] A. Patel, H. O. Lee, L. Jawerth, S. Maharana, M. Jahnel, M. Y. Hein, S. Stoynov, J. Mahamid, S. Saha, T. M. Franzmann, A. Pozniakovski, I. Poser, N. Maghelli, L. A. Royer, M. Weigert, E. W. Myers, S. Grill, D. Drechsel, A. A. Hyman, S. Alberti, *Cell* **2015**, *162*, 1066–1077.
[24] K. A. Burke, A. M. Janke, C. L. Rhine, N. L. Fawzi, *Mol. Cell* **2015**, *60*, 231–241.
[25] C. M. Dewey, B. Cenik, C. F. Sephton, B. A. Johnson, J. Herz, G. Yu, *Brain Res.* **2012**, *1462*, 16–25.
[26] L. Streit, T. Kuhn, T. Vomhof, V. Bopp, A. C. Ludolph, J. H. Weishaupt, J. C. M. Gebhardt, J. Michaelis, K. M. Danzer, *Nat. Commun.* **2022**, *13*, 5480.
[27] B. Das, S. Roychowdhury, P. Mohanty, A. Rizuan, J. Chakraborty, J. Mittal, K. Chattopadhyay, *EMBO J.* **2023**, *42*, e111185.
[28] J. Gal, L. Kuang, K. R. Barnett, B. Z. Zhu, S. C. Shissler, K. V. Korotkov, L. J. Hayward, E. J. Kasarskis, H. Zhu, *Acta Neuropathol.* **2016**, *132*, 563–576.
[29] D.-Y. Lee, G. S. Jeon, J.-J. Sung, *Neurochem. Res.* **2020**, *45*, 2884–2893.
[30] A. Molliex, J. Temirov, J. Lee, M. Coughlin, A. P. Kanagaraj, H. J. Kim, T. Mittag, J. P. Taylor, *Cell* **2015**, *163*, 123–133.
[31] S. Ray, T. O. Mason, L. Boyens-Thiele, A. Farzadfard, J. A. Larsen, R. K. Norrild, N. Jahnke, A. K. Buell, *Nat. Chem.* **2023**, *15*, 1306–1316.
[32] N. Younas, S. Zafar, T. Saleem, L. C. Fernandez Flores, A. Younas, M. Schmitz, I. Zerr, *Cell Biosci.* **2023**, *13*, 221.
[33] H. Zhang, X. Ji, P. Li, C. Liu, J. Lou, Z. Wang, W. Wen, Y. Xiao, M. Zhang, X. Zhu, *Sci. China Life Sci.* **2020**, *63*, 953–985.
[34] M. Poudyal, K. Patel, L. Gadhe, A. S. Sawner, P. Kadu, D. Datta, S. Mukherjee, S. Ray, A. Navalkar, S. Maiti, D. Chatterjee, J. Devi, R. Bera, N. Gahlot, J. Joseph, R. Padinhateeri, S. K. Maji, *Nat. Commun.* **2023**, *14*, 6199.
[35] X. Gui, S. Feng, Z. Li, Y. Li, B. Reif, B. Shi, Z. Niu, *J. Biol. Chem.* **2023**, *299*, 102926.
[36] W. P. Lipiński, B. S. Visser, I. Robu, M. A. A. Fakhree, S. Lindhoud, M. M. A. E. Claessens, E. Spruijt, *Sci. Adv.* **2022**, *8*, eabq6495.
[37] T. E. Audas, D. E. Audas, M. D. Jacob, J. J. D. Ho, M. Khacho, M. Wang, J. K. Perera, C. Gardiner, C. A. Bennett, T. Head, O. N. Kryvenko, M. Jorda, S. Daunert, A. Malhotra, L. Trinkle-Mulcahy, M. L. Gonzalgo, S. Lee, *Dev. Cell* **2016**, *39*, 155–168.
[38] A. M. Küffner, M. Linsenmeier, F. Grigolato, M. Prodan, R. Zuccarini, U. Capasso Palmiero, L. Faltova, P. Arosio, *Chem. Sci.* **2021**, *12*, 4373–4382.
[39] E. W. Martin, T. S. Harmon, J. B. Hopkins, S. Chakravarthy, J. J. Incicco, P. Schuck, A. Soranno, T. Mittag, *Nat. Commun.* **2021**, *12*, 4513.
[40] X. Zeng, A. S. Holehouse, A. Chilkoti, T. Mittag, R. V. Pappu, *Biophys. J.* **2020**, *119*, 402–418.
[41] J. Berry, C. P. Brangwynne, M. Haataja, *Rep. Prog. Phys.* **2018**, *81*, 046601.
[42] A. Narayanan, A. Meriin, J. O. Andrews, J.-H. Spille, M. Y. Sherman, I. I. Cisse, *eLife* **2019**, *8*, e39695.
[43] S. T. Dada, M. C. Hardenberg, Z. Toprakcioglu, L. K. Mrugalla, M. P. Cali, M. O. McKeon, E. Klimont, T. C. T. Michaels, T. P. J. Knowles, M. Vendruscolo, *Proc. Nat. Acad. Sci.* **2023**, *120*, e2208792120.
[44] S. F. Banani, H. O. Lee, A. A. Hyman, M. K. Rosen, *Nat. Rev. Mol. Cell Biol.* **2017**, *18*, 285–298.
[45] A. C. Murthy, N. L. Fawzi, *J. Biol. Chem.* **2020**, *295*, 2375–2384.
[46] J. E. Bramham, A. P. Golovanov, *Nat. Commun.* **2022**, *13*, 1767.
[47] M. P. Hughes, M. R. Sawaya, D. R. Boyer, L. Goldschmidt, J. A. Rodriguez, D. Cascio, L. Chong, T. Gonen, D. S. Eisenberg, *Science* **2018**, *359*, 698–701.


© 2024 The Authors. Chemistry - A European Journal published by Wiley-VCH GmbH

[48] T. Scheidt, U. Łapińska, J. R. Kumita, D. R. Whiten, D. Klenerman, M. R. Wilson, S. I. A. Cohen, S. Linse, M. Vendruscolo, C. M. Dobson, T. P. J. Knowles, P. Arosio, *Sci. Adv.* **2019**, *5*, eaau3112..

[49] T. C. T. Michaels, A. Šarić, S. Curk, K. Bernfur, P. Arosio, G. Meisl, A. J. Dear, S. I. A. Cohen, C. M. Dobson, M. Vendruscolo, S. Linse, T. P. J. Knowles, *Nat. Chem.* **2020**, *12*, 445–451.

[50] R. Morales, J. Bravo-Alegria, C. Duran-Aniotz, C. Soto, *Sci. Rep.* **2015**, *5*, 9349.

[51] R. F. Rosen, J. J. Fritz, J. Dooyema, A. F. Cintron, T. Hamaguchi, J. J. Lah, H. LeVine, M. Jucker, L. C. Walker, *J. Neurochem.* **2012**, *120*, 660–666.

[52] R. F. Sowade, T. R. Jahn, *Nat. Commun.* **2017**, *8*, 512.

[53] A. K. Buell, in *Int. Rev. Cell Mol. Biol.*, Elsevier, **2017**, pp. 187–226.

[54] S. I. A. Cohen, S. Linse, L. M. Luheshi, E. Hellstrand, D. A. White, L. Rajah, D. E. Otzen, M. Vendruscolo, C. M. Dobson, T. P. J. Knowles, *Proc. Nat. Acad. Sci.* **2013**, *110*, 9758–9763.

[55] A. K. Buell, *Biochem. J.* **2019**, *476*, 2677–2703.

[56] K. Brännström, T. Islam, A. L. Gharibyan, I. Iakovleva, L. Nilsson, C. C. Lee, L. Sandblad, A. Pamrén, A. Olofsson, *J. Mol. Biol.* **2018**, *430*, 1940–1949.

[57] N. Vettore, A. K. Buell, *Phys. Chem. Chem. Phys.* **2019**, *21*, 26184–26194.

[58] S. I. A. Cohen, R. Cukalevski, T. C. T. Michaels, A. Šarić, M. Törnquist, M. Vendruscolo, C. M. Dobson, A. K. Buell, T. P. J. Knowles, S. Linse, *Nat. Chem.* **2018**, *10*, 523–531.

[59] L. Hou, M. G. Zagorski, *J. Am. Chem. Soc.* **2006**, *128*, 9260–9261.

[60] Y. Miller, B. Ma, R. Nussinov, *Proc. Nat. Acad. Sci.* **2010**, *107*, 9490–9495.

[61] D. P. Smith, D. G. Smith, C. C. Curtain, J. F. Boas, J. R. Pilbrow, G. D. Ciccotosto, T.-L. Lau, D. J. Tew, K. Perez, J. D. Wade, A. I. Bush, S. C. Drew, F. Separovic, C. L. Masters, R. Cappai, K. J. Barnham, *J. Biol. Chem.* **2006**, *281*, 15145–15154.

[62] S. Parthasarathy, F. Long, Y. Miller, Y. Xiao, D. McElheny, K. Thurber, B. Ma, R. Nussinov, Y. Ishii, *J. Am. Chem. Soc.* **2011**, *133*, 3390–3400.

[63] E. J. Crooks, B. A. Irizarry, M. Ziliox, T. Kawakami, T. Victor, F. Xu, H. Hojo, K. Chiu, C. Simmerling, W. E. Van Nostrand, S. O. Smith, L. M. Miller, *J. Biol. Chem.* **2020**, *295*, 8914–8927.

[64] Z. Niu, W. Zhao, Z. Zhang, F. Xiao, X. Tang, J. Yang, *Angew. Chem. Int. Ed.* **2014**, *53*, 9294–9297.

[65] M. Bokvist, F. Lindström, A. Watts, G. Gröbner, *J. Mol. Biol.* **2004**, *335*, 1039–1049.

[66] S. A. Kotler, P. Walsh, J. R. Brender, A. Ramamoorthy, *Chem. Soc. Rev.* **2014**, *43*, 6692–6700.

[67] Z. Niu, Z. Zhang, W. Zhao, J. Yang, *Biochim. Biophys. Acta Biomembr.* **2018**, *1860*, 1663–1669.

[68] H. Fatafta, M. Khaled, M. C. Owen, A. Sayyed-Ahmad, B. Strodel, *Proc. Nat. Acad. Sci.* **2021**, *118*, e2106210118.

[69] Q. Cheng, Z.-W. Hu, K. E. Doherty, Y. J. Tobin-Miyaji, W. Qiang, *Biochim. Biophys. Acta Biomembr.* **2018**, *1860*, 1670–1680.

[70] P. Flagmeier, S. De, T. C. T. Michaels, X. Yang, A. J. Dear, C. Emanuelsson, M. Vendruscolo, S. Linse, D. Klenerman, T. P. J. Knowles, C. M. Dobson, *Nat. Struct. Mol. Biol.* **2020**, *27*, 886–891.

[71] A. Wang, A. E. Conicella, H. B. Schmidt, E. W. Martin, S. N. Rhoads, A. N. Reeb, A. Nourse, D. Ramirez Montero, V. H. Ryan, R. Rohatgi, F. Shewmaker, M. T. Naik, T. Mittag, Y. M. Ayala, N. L. Fawzi, *EMBO J.* **2018**, *37*, e97452.

[72] M. R. Marzahn, S. Marada, J. Lee, A. Nourse, S. Kenrick, H. Zhao, G. Ben-Nissan, R. Kolaitis, J. L. Peters, S. Pounds, W. J. Errington, G. G. Privé, J. P. Taylor, M. Sharon, P. Schuck, S. K. Ogden, T. Mittag, *EMBO J.* **2016**, *35*, 1254–1275.

[73] R. Tycko, *Neuron* **2015**, *86*, 632–645.

[74] J. Adamcik, R. Mezzenga, *Angew. Chem. Int. Ed.* **2018**, *57*, 8370–8382.

[75] J. Gath, L. Bousset, B. Habenstein, R. Melki, B. H. Meier, A. Böckmann, *Biomol. NMR Assign.* **2014**, *8*, 395–404.

[76] M. D. Tuttle, G. Comellas, A. J. Nieuwkoop, D. J. Covell, D. A. Berthold, K. D. Kloepper, J. M. Courtney, J. K. Kim, A. M. Barclay, A. Kendall, W. Wan, G. Stubbs, C. D. Schwieters, V. M. Y. Lee, J. M. George, C. M. Rienstra, *Nat. Struct. Mol. Biol.* **2016**, *23*, 409–415.

[77] J. Zhao, X. Yu, G. Liang, J. Zheng, *Biomacromolecules* **2011**, *12*, 210–220.

[78] C. Röder, T. Kupreichyk, L. Gremer, L. U. Schäfer, K. R. Pothula, R. B. G. Ravelli, D. Willbold, W. Hoyer, G. F. Schröder, *Nat. Struct. Mol. Biol.* **2020**, *27*, 660–667.

[79] M. R. Sawaya, S. Sambashivan, R. Nelson, M. I. Ivanova, S. A. Sievers, M. I. Apostol, M. J. Thompson, M. Balbirnie, J. J. W. Wiltzius, H. T. McFarlane, A. Ø. Madsen, C. Riekel, D. Eisenberg, *Nature* **2007**, *447*, 453–457.

[80] J.-P. Colletier, A. Laganowsky, M. Landau, M. Zhao, A. B. Soriaga, L. Goldschmidt, D. Flot, D. Cascio, M. R. Sawaya, D. Eisenberg, *Proc. Nat. Acad. Sci.* **2011**, *108*, 16938–16943.

[81] J. A. Rodriguez, M. I. Ivanova, M. R. Sawaya, D. Cascio, F. E. Reyes, D. Shi, S. Sangwan, E. L. Guenther, L. M. Johnson, M. Zhang, L. Jiang, M. A. Arbing, B. L. Nannenga, J. Hattne, J. Whitelegge, A. S. Brewster, M. Messerschmidt, S. Boutet, N. K. Sauter, T. Gonen, D. S. Eisenberg, *Nature* **2015**, *525*, 486–490.

[82] C. Nguyen, T. Gonen, *Curr. Opin. Struct. Biol.* **2020**, *64*, 51–58.

[83] P. Krotee, S. L. Griner, M. R. Sawaya, D. Cascio, J. A. Rodriguez, D. Shi, S. Philipp, K. Murray, L. Saelices, J. Lee, P. Seidler, C. G. Glabe, L. Jiang, T. Gonen, D. S. Eisenberg, *J. Biol. Chem.* **2018**, *293*, 2888–2902.

[84] R. A. Warmack, D. R. Boyer, C.-T. Zee, L. S. Richards, M. R. Sawaya, D. Cascio, T. Gonen, D. S. Eisenberg, S. G. Clarke, *Nat. Commun.* **2019**, *10*, 3357.

[85] R. Riek, *Cold Spring Harbor Perspect. Biol.* **2017**, *9*, a023572.

[86] M. Ahmed, J. Davis, D. Aucoin, T. Sato, S. Ahuja, S. Aimoto, J. I. Elliott, W. E. Van Nostrand, S. O. Smith, *Nat. Struct. Mol. Biol.* **2010**, *17*, 561–567.

[87] Y. Xiao, I. Matsuda, M. Inoue, T. Sasahara, M. Hoshi, Y. Ishii, *J. Biol. Chem.* **2020**, *295*, 458–467.

[88] M. A. Kostylev, M. D. Tuttle, S. Lee, L. E. Klein, H. Takahashi, T. O. Cox, E. C. Gunther, K. W. Zilm, S. M. Strittmatter, *Mol. Cell* **2018**, *72*, 426–443. e12.

[89] L. Amin, D. A. Harris, *Nat. Commun.* **2021**, *12*, 3451.

[90] A. S. König, N. S. Rösener, L. Gremer, M. Tusche, D. Flender, E. Reinartz, W. Hoyer, P. Neudecker, D. Willbold, H. Heise, *J. Biol. Chem.* **2021**, *296*, 100499..

[91] J. Wu, T. B. Blum, D. P. Farrell, F. DiMaio, J. P. Abrahams, J. Luo, *Angew. Chem. Int. Ed.* **2021**, *60*, 18680–18687.

[92] S. Ciudad, E. Puig, T. Botzanowski, M. Meigooni, A. S. Arango, J. Do, M. Mayzel, M. Bayoumi, S. Chaignepain, G. Maglia, S. Cianferani, V. Orekhov, E. Tajkhorshid, B. Bardiaux, N. Carulla, *Nat. Commun.* **2020**, *11*, 3014.

[93] P. Liu, M. N. Reed, L. A. Kotilinek, M. K. O. Grant, C. L. Forster, W. Qiang, S. L. Shapiro, J. H. Reichl, A. C. A. Chiang, J. L. Jankowsky, C. M. Wilmot, J. P. Cleary, K. R. Zahs, K. H. Ashe, *Cell Rep.* **2015**, *11*, 1760–1771.

[94] A. K. Paravastu, R. D. Leapman, W.-M. Yau, R. Tycko, *Proc. Nat. Acad. Sci.* **2008**, *105*, 18349–18354.

[95] J. A. Raskatov, A. R. Foley, J. M. Louis, W.-M. Yau, R. Tycko, *J. Am. Chem. Soc.* **2021**, *143*, 13299–13313.

[96] N. G. Sgourakis, W.-M. Yau, W. Qiang, *Structure* **2015**, *23*, 216–227.

[97] W. Qiang, W.-M. Yau, Y. Luo, M. P. Mattson, R. Tycko, *Proc. Nat. Acad. Sci.* **2012**, *109*, 4443–4448.

[98] A. K. Schütz, T. Vagt, M. Huber, O. Y. Ovchinnikova, R. Cadalbert, J. Wall, P. Güntert, A. Böckmann, R. Glockshuber, B. H. Meier, *Angew. Chem. Int. Ed.* **2015**, *54*, 331–335.

[99] J.-X. Lu, W. Qiang, W.-M. Yau, C. D. Schwieters, S. C. Meredith, R. Tycko, *Cell* **2013**, *154*, 1257–1268.

[100] U. Ghosh, K. R. Thurber, W.-M. Yau, R. Tycko, *Proc. Nat. Acad. Sci.* **2021**, *118*, e2023089118.

[101] U. Ghosh, W.-M. Yau, J. Collinge, R. Tycko, *Proc. Nat. Acad. Sci.* **2021**, *118*, e2111863118.

[102] M. Kollmer, W. Close, L. Funk, J. Rasmussen, A. Bsoul, A. Schierhorn, M. Schmidt, C. J. Sigurdson, M. Jucker, M. Fändrich, *Nat. Commun.* **2019**, *10*, 4760.

[103] M. A. Wälti, F. Ravotti, H. Arai, C. G. Glabe, J. S. Wall, A. Böckmann, P. Güntert, B. H. Meier, R. Riek, *Proc. Nat. Acad. Sci.* **2016**, *113*, E4976–E4984.

[104] M. T. Colvin, R. Silvers, Q. Z. Ni, T. V. Can, I. Sergeyev, M. Rosay, K. J. Donovan, B. Michael, J. Wall, S. Linse, R. G. Griffin, *J. Am. Chem. Soc.* **2016**, *138*, 9663–9674.

[105] Y. Xiao, B. Ma, D. McElheny, S. Parthasarathy, F. Long, M. Hoshi, R. Nussinov, Y. Ishii, *Nat. Struct. Mol. Biol.* **2015**, *22*, 499–505.

[106] A. Wickramasinghe, Y. Xiao, N. Kobayashi, S. Wang, K. P. Scherpelz, T. Yamazaki, S. C. Meredith, Y. Ishii, *J. Am. Chem. Soc.* **2021**, *143*, 11462–11472.

[107] M. Schmidt, A. Rohou, K. Lasker, J. K. Yadav, C. Schiene-Fischer, M. Fändrich, N. Grigorieff, *Proc. Nat. Acad. Sci.* **2015**, *112*, 11858–11863.

[108] L. Gremer, D. Schölzel, C. Schenk, E. Reinartz, J. Labahn, R. B. G. Ravelli, M. Tusche, C. Lopez-Iglesias, W. Hoyer, H. Heise, D. Willbold, G. F. Schröder, *Science* **2017**, *358*, 116–119.

[109] Y. Yang, D. Arseni, W. Zhang, M. Huang, S. Lövestam, M. Schweighauser, A. Kotecha, A. G. Murzin, S. Y. Peak-Chew, J. Macdonald, I. Lavenir, H. J. Garringer, E. Gelpi, K. L. Newell, G. G. Kovacs, R. Vidal, B.



© 2024 The Authors. Chemistry - A European Journal published by Wiley-VCH GmbH

Ghetti, B. Ryskeldi-Falcon, S. H. W. Scheres, M. Goedert, *Science* **2022**, *375*, 167–172.
[110] L. Cerofolini, E. Ravera, S. Bologna, T. Wiglenda, A. Böddrich, B. Purfürst, I. Benilova, M. Korsak, G. Gallo, D. Rizzo, L. Gonnelli, M. Fragai, B. De Strooper, E. E. Wanker, C. Luchinat, *Chem. Commun.* **2020**, *56*, 8830–8833.
[111] U. Cendrowska, P. J. Silva, N. Ait-Bouziad, M. Müller, Z. P. Guven, S. Vieweg, A. Chiki, L. Radamaker, S. T. Kumar, M. Fändrich, F. Tavanti, M. C. Menziani, A. Alexander-Katz, F. Stellacci, H. A. Lashuel, *Proc. Nat. Acad. Sci.* **2020**, *117*, 6866–6874.
[112] J. Zhou, L. Venturelli, L. Keiser, S. K. Sekatskii, F. Gallaire, S. Kasas, G. Longo, T. P. J. Knowles, F. S. Ruggeri, G. Dietler, *ACS Nano* **2021**, *15*, 944–953..
[113] E. F. Pettersen, T. D. Goddard, C. C. Huang, G. S. Couch, D. M. Greenblatt, E. C. Meng, T. E. Ferrin, *J. Comput. Chem.* **2004**, *25*, 1605–1612.

Manuscript received: January 22, 2024
Accepted manuscript online: June 18, 2024
Version of record online: August 2, 2024


© 2024 The Authors. Chemistry - A European Journal published by Wiley-VCH GmbH